Macromolecule-like Aspects for a Colloidal Suspension of an Exfoliated Titanate. Pairwise Association of Nanosheets and Dynamic Reassembling Process Initiated from It

Takayoshi Sasaki,* Mamoru Watanabe, Hideo Hashizume, Hirohisa Yamada, and Hiromoto Nakazawa

Contribution from the National Institute for Research in Inorganic Materials, 1-1 Namiki, Tsukuba, Ibaraki 305, Japan

Received January 9, 1996[⊗]

Abstract: A layered protonic titanate of lepidocrocite-type, $H_xTi_{2-x/4}\square_{x/4}O_4 \cdot H_2O$ ($x \sim 0.7$; □, vacancy), has been exfoliated on the action of an aqueous solution of tetrabutylammonium (hereafter TBA) hydroxide, which resulted in a stable colloidal suspension. A colloidal aggregate centrifuged from the suspension was examined by an in situ X-ray diffraction technique under conditions where drying speed was controlled. The diffraction immediately after separation from the liquid phase was principally amorphous except for a series of sharp reflections detected in a small angle scattering region. On the basis of the line profile analysis, the latter diffraction feature was accounted for by the fundamental intersheet interference of a spacing >10 nm, which demonstrates the existence of a novel associated pair of the titanate nanosheets accommodating a large volume of water cluster between them. These XRD data provide persuasive evidence for delamination into single layers. Upon drying, the amorphous halo disappeared and changed into a well-ordered crystalline pattern. This can be explained by reassembling of the individual sheets which was initiated from the paired species. A TBA intercalated compound was finally obtained as a result of drying. The theoretical simulations on the XRD data revealed that the process involves increase of the crystallites which grows in number of the sheets but shrinks in terms of intersheet distance. The dynamic process from the colloidal nanosheets to the restacked layered structure was followed here for the first time, which throws light upon the inherent nature of "single-layer colloidal suspensions" as inorganic macromolecules.

Introduction

It is well-known that some clay minerals spontaneously undergo delamination in water to produce "single-layer colloidal suspensions". Recently it has been reported that similar exfoliation can be artificially achieved for several classes of layered materials by some soft-chemical procedures.[1] Resulting suspensions have attracted considerable attention both from fundamental and practical veiwpoints. Exfoliated single layers are expected to behave as a new kind of inorganic macromolecule which may exhibit some unique properties different from those of bulk materials. Novel materials, thin films, and organic/inorganic nanocomposites have been fabricated from them.[2−12] Most recently, they have been reported to be used as building blocks to construct self-assembly multilayers.[13,14]

Despite their importance, the nature of the suspensions as well as the degree of delamination has not been fully understood, mainly due to lack of appropriate characterizations. "Single-layer colloids" have been examined mostly by TEM observations, some of which are combined with platinum shadowing by low-angle deposition techniques or with measurements of Rutherford scattered intensities.[15−17] They found some distribution of stacked multiple sheets as well as single layers. It is to be pointed out that TEM is inevitably concerned with dried products, which may not be a perfect reflection of the natural state in suspensions. Therefore, it is preferable to study "single-layer colloids" as they are since they, especially for layered compounds with high charge density, tend to be restacked on drying. Joensen *et al*. have reported some X-ray diffraction (XRD) studies on an exfoliated MoS_2 and its related materials in its wet state.[18] They have discussed the existence of a single molecular sheet of the chalcogenides on the basis of the line profile of intrasheet diffraction, but they did not pay attention to small-angle scattering, which may be of relevance in obtaining the information on sheet-to-sheet interaction.

[⊗] Abstract published in *Advance ACS Abstracts,* August 1, 1996.

(1) Jacobson, A. J. *Mater. Sci. Forum* **1994**, *152−153*, 1−12.
(2) Alberti, G.; Casciola, M.; Costantino, U. *J. Colloid Interface Sci.* **1985**, *107*, 256−263.
(3) Divigalpitiya, W. M. R.; Frindt, R. F.; Morrison, S. R. *Science* **1989**, *246*, 369−371.
(4) Miremadi, B. K.; Morrison, S. R. *J. Appl. Phys.* **1990**, *67*, 1515−1520.
(5) Nazar, L. F.; Liblong, S. W.; Yin, X. T. *J. Am. Chem. Soc.* **1991**, *113*, 5889−5890.
(6) Divigalpitiya, W. M. R.; Frindt, R. F.; Morrison, S. R. *J. Mater. Res.* **1991**, *6*, 1103−1107.
(7) Kanatzidis, M. G.; Bissessur, R.; DeGroot, D. C.; Schindler, J. L.; Kannewurf, C. R. *Chem. Mater.* **1993**, *5*, 595−596.
(8) Lemmon, J. P.; Lerner, M. M. *Chem. Mater.* **1994**, *6*, 207−210.
(9) Guay, D.; Divigalpitiya, W. M. R.; Bélanger, D.; Feng, X. H. *Chem. Mater.* **1994**, *6*, 614−619.
(10) (a) Manivannan, A.; Santiago, Y.; Cabrera, C. R. *J. Vac. Sci. Technol. B* **1994**, *12*, 2111−2114. (b) Santiago, Y.; Cabrera, C. R. *J. Electrochem. Soc.* **1994**, *141*, 629−635.
(11) Yang, D.; Frindt, R. F. *Mol. Cryst. Liq. Cryst.* **1994**, *244*, 355−360.
(12) Foglia, S.; Tomlinson, A. A. G.; Mulley, S.; Sironi, A. *J. Mater. Chem.* **1995**, *5*, 1191−1196.
(13) Kleinfield, E. R.; Ferguson, G. S. *Science* **1994**, *265*, 370−373.
(14) Keller, S. W.; Kim, H.-N.; Mallouk, T. E. *J. Am. Chem. Soc.* **1994**, *116*, 8817−8818.
(15) (a) Nadeau, P. H.; Wilson, M. J.; McHardy, W. J.; Tait, J. M. *Science* **1984**, *225*, 923−925. (b) Nadeau, P. H.; Wilson, M. J.; McHardy, W. J.; Tait, J. M. *Clay Miner.* **1984**, *19*, 67−76. (c) Nadeau, P. H.; Wilson, M. J.; McHardy, W. J.; Tait, J. M. *Clay Miner.* **1984**, *19*, 757−769.
(16) Bonneau, P.; Mansot, J. L.; Rouxel, J. *Mater. Res. Bull.* **1993**, *28*, 757−766.
(17) Treacy, M. M. J.; Rice, S. B.; Jacobson, A. J.; Lewandowski, J. T. *Chem. Mater.* **1990**, *2*, 279−286.
(18) (a) Liu, C.; Singh, O.; Joensen, P.; Curzon, A. E.; Frindt, R. F. *Thin Solid Films* **1984**, *113*, 165−172. (b) Joensen, P.; Frindt, R. F.; Morrison, S. R. *Mater. Res. Bull.* **1986**, *21*, 457−461. (c) Joensen, P.; Crozier, E. D.; Alberding, N.; Frindt, R. F. *J. Phys. C: Solid State Phys.* **1987**, *20*, 4043−4053. (d) Yang, D.; Jiménez Sandoval, S.; Divigalpitiya, W. M. R.; Irwin, J. C.; Frindt, R. F. *Phys. Rev. B* **1991**, *43*, 12053−12056.

S0002-7863(96)00073-X CCC: $12.00

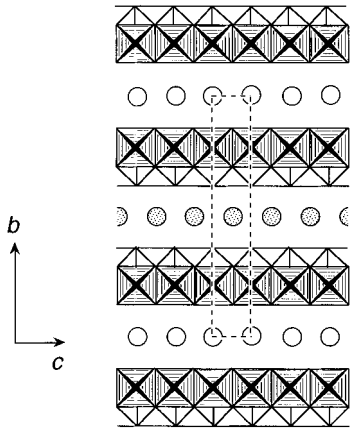

Figure 1. Schematic representation of the crystal structure for the protonic titanate $H_xTi_{2-x/4}\square_{x/4}O_4{\cdot}H_2O$ viewed down along the *a* axis. The compound crystallizes as a body-centered orthorhombic system (*Immm*) with cell parameters of $a = 0.3783(2)$ nm, $b = 1.8735(8)$ nm, and $c = 0.2978(2)$ nm (for $x = 0.7$ material).[22] The host layer is of lepidocrocite-type in which TiO_6 octahedra are combined via edge sharing to produce a two-dimensional sheet of composition $Ti_{2-x/4}\square_{x/4}O_4^{x-}$. Open and stippled circles designate interlayer water molecules at $x = 0$ and $^1/_2$, respectively, 70% of which are protonated. A minus charge, as a consequence of Ti site vacancy, is compensated for by the interlayer oxonium ions.

In this paper, we present in situ XRD data, especially focussing on those at a low angular range, for a colloidal suspension of an exfoliated titanate to get insight into the inherent nature of "single-layer colloids". A variety of layered titanates, $H_2Ti_3O_7$, $H_2Ti_4O_9{\cdot}1.2H_2O$, $H_2Ti_5O_{11}{\cdot}3H_2O$, and $H_xTi_{2-x/4}\square_{x/4}O_4{\cdot}H_2O$ ($x \sim 0.7$; $\square$, vacancy), have been synthesized in protonic forms[19−22] and their ion-exchange and intercalation properties have been studied extensively.[23−29] However, there have been few reports on exfoliation of these materials. A single-layer titanate will be attractive because of prospects for unusual optical properties, highly active photocatalytic actions, and so on. The protonic titanate, $H_xTi_{2-x/4}\square_{x/4}O_4{\cdot}H_2O$,[22] with a lepidocrocite-like layered structure (see Figure 1), was chosen since its exfoliation is expected to be most feasible. The electrostatic interlayer interaction is the weakest due to its lowest charge density in comparison with the others.[22] Separation into single sheets (nanosheets[30]) and their macromolecule-like behavior in the reassembling process were demonstrated.

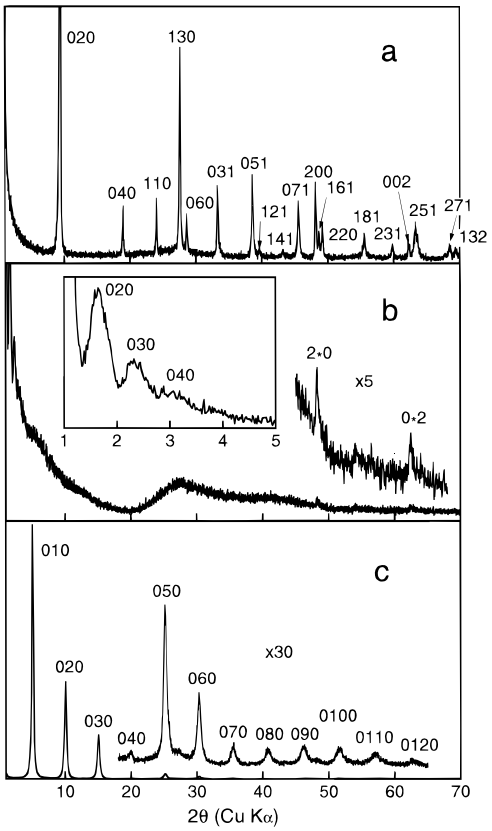

Figure 2. X-ray diffraction patterns before and after the exfoliation: (a) a polycrystalline sample of $H_xTi_{2-x/4}\square_{x/4}O_4{\cdot}H_2O$ and (b) a wet colloidal aggregate centrifuged from the exfoliated titanate suspension (the detailed pattern at a low angular range is in inset) and (c) dried for 1 h at a relatively humidity of 20% and temperature of 30 °C. The intensity scale in c is 20 times that in b.

Results

In Situ X-ray Diffraction. Changes in XRD data during exfoliation and subsequent reassembling processes are summarized in Figure 2. The data for $H_xTi_{2-x/4}\square_{x/4}O{\cdot}H_2O$ before delamination (Figure 2a) are consistent with those of the body-centered orthorhombic structure with the interlayer distance of 0.94 nm shown in Figure 1.

A stable colloidal suspension was obtained by treating the protonic oxide with a TBA hydroxide solution. A colloidal aggregate centrifuged from the suspension of typical composition (0.4 wt %, 5-fold excess of TBA ions over exchangeable protons in the titanate) was subjected to XRD measurements under the humid condition (relative humidity 95%, temperature 30 °C) where drying is suppressed. The diffraction pattern for the wet colloidal aggregate is characterized, for the most part, by amorphouslike one (see Figure 2b), which should be interpreted as a combination of scattering from water and the titanate. Disappearance of the sharp diffraction pattern in Figure 2a confirms that the layered structure was collapsed.

Besides the broad character, two noticeable features can be discerned. One is faint reflections at the 2θ values of ~48°

(19) (a) Izawa, H.; Kikkawa, S.; Koizumi, M. *J. Phys. Chem.* **1982**, *86*, 5023−5026. (b) Feist, T. P.; Mocarski, S. J.; Davies, P. K.; Jacobson, A. J.; Lewandowski, J. T. *Solid State Ionics* **1988**, *28*−*30*, 1338−1343. (c) Feist, T. P.; Davies, P. K. *J. Solid State Chem.* **1992**, *101*, 275−295.

(20) (a) Marchand, R.; Brohan, L.; Tournoux, M. *Mater. Res. Bull.* **1980**, *15*, 1129−1133. (b) Sasaki, T.; Watanabe, M.; Komatsu, Y.; Fujiki, Y. *Inorg. Chem.* **1985**, *24*, 2265−2271.

(21) Sasaki, T.; Komatsu, Y.; Fujiki, Y. *Chem. Mater.* **1992**, *4*, 894−899.

(22) (a) Sasaki, T.; Komatsu, Y.; Fujiki, Y. *J. Chem. Soc., Chem. Commun.* **1991**, 817−818. (b) Sasaki, T.; Watanabe, M.; Michiue, Y.; Komatsu, Y.; Izumi, F.; Takenouchi, S. *Chem. Mater.* **1995**, *7*, 1001−1007.

(23) (a) Izawa, H.; Kikkawa, S.; Koizumi, M. *J. Solid State Chem.* **1985**, *60*, 264−267. (b) Izawa, H.; Kikkawa, S.; Koizumi, M. *J. Solid State Chem.* **1987**, *69*, 336−342.

(24) (a) Sasaki, T.; Watanabe, M.; Komatsu, Y.; Fujiki, Y. *Bull. Chem. Soc. Jpn.* **1985**, *58*, 3500−3505. (b) Sasaki, T.; Komatsu, Y.; Fujiki, Y. *Mater. Res. Bull.* **1987**, *22*, 1321−1328. (c) Sasaki, T.; Komatsu, Y.; Fujiki, Y. *Inorg. Chem.* **1989**, *28*, 2776−2779.

(25) (a) Anderson, M. W.; Klinowski, J. *Inorg. Chem.* **1990**, *29*, 3260−3263. (b) Landis, M. E.; Aufdembrink, B. A.; Chu, P.; Johnson, I. D.; Kirker, G. W.; Rubin, M. K. *J. Am. Chem. Soc.* **1991**, *113*, 3189−3190.

(26) (a) Cheng, S.; Wang, T. *Inorg. Chem.* **1989**, *28*, 1283−1289. (b) Sylvester, P.; Cahill, R.; Clearfield, A. *Chem. Mater.* **1994**, *6*, 1890−1898. (c) Hou, W.; Yan, Q.; Peng, B.; Fu, X. *J. Mater. Chem.* **1995**, *5*, 109−114.

(27) Izawa, H.; Kikkawa, S.; Koizumi, M. *Polyhedron* **1983**, *2*, 741−744.

(28) (a) Clément, P.; Marchand, R. *C. R. Acad. Sci. Paris Ser. II* **1983**, *296*, 1161−1164. (b) Miyata, H.; Sugahara, Y.; Kuroda, K.; Kato, C. *J. Chem. Soc., Faraday Trans. 1* **1988**, *84*, 2677−2682.

(29) Sasaki, T.; Izumi, F.; Watanabe, M. *Chem. Mater.* **1996**, *8*, 777−782.

(30) We use this term "nanosheet" for the individual host layers, the thickness of which is approximately 0.75 nm (see Figure 1). The lateral dimension was in a range of 0.3−1.0 μm for the material used in this study, which should be dependent on preparation modes of the parent Cs compound.

and ~62°. These two can be indexed as 2∗0 and 0∗2, respectively, giving unit periodicities of the host layer illustrated in Figure 1. The asymmetric line shape with a tail toward the higher angle side is characteristic of diffraction from a two-dimensional lattice. This indicates that the covalent framework consisted of titanium and oxygen was preserved even in the colloid.

The other feature is a series of sharp peaks in a very low angular range as emphasized by the inset. Their spacings were 5.4, 3.8, and 2.9 nm, which means that these are assignable as 020, 030, and 040 reflections,[31] respectively, of a spacing as large as 11−12 nm. This diffraction can be elucidated by stacking of the nanosheets, which will be described below. In summary, the XRD data strongly suggest that the layered structure was exfoliated to the individual nanosheets, a small portion of which are stacked to give the small-angle scattering.

On drying, the amorphous diffraction pattern changed into a very crystalline one as depicted in Figure 2c. This indicates that almost all of the delaminated sheets were restacked again. The reassembling process will also be detailed below.

Diffraction Profile Analysis. It is intriguing to clarify what species gave the small-angle scattering (inset of Figure 2b) which was indicative of the exceptionally large spacing of >10 nm. The oscillating profile without a flat region between the lines implies that only a very limited number of nanosheets were stacked. In order to obtain accurate information, the 0*k*0 diffraction patterns were numerically simulated for the system of N parallel nanosheets with the spacing of d_{010} using the following equations.

$$I(\theta) = \frac{1+\cos^2 2\theta}{\sin^2\theta\cos\theta}\cdot F^2(\theta)\cdot\frac{\sin^2(2\pi N d_{010}\sin\theta/\lambda)}{\sin^2(2\pi d_{010}\sin\theta/\lambda)} \qquad (1)$$

where the first, second, and third terms are the Lorentz−polarization factor, structure factor, and interference function, respectively. The notations, θ and λ, are the scattering angle and wavelength of the X-ray, respectively. The structure factor was calculated as follows on the basis of the model illustrated in Figure 3.

$$\begin{aligned} F(\theta) = {} & 2\int_0^{d_w/2}(f_O/0.25)\cdot\cos 2\pi(2y\cdot\sin\theta/\lambda)\,dy \\ & + 2\cdot 0.9125 f_{Ti}\cos 2\pi[2(d_{010}/2 - 0.075)\cdot\sin\theta/\lambda]\cdot \\ & \quad \exp[-B_{Ti}\cdot(\sin\theta/\lambda)^2] \\ & + 2f_O\cos 2\pi[2(d_{010}/2 - 0.225)\cdot\sin\theta/\lambda]\cdot \\ & \quad \exp[-B_O\cdot(\sin\theta/\lambda)^2] \\ & + 2f_O\cos 2\pi[2(d_{010}/2 - 0.075)\cdot\sin\theta/\lambda]\cdot \\ & \quad \exp[-B_O\cdot(\sin\theta/\lambda)^2] \end{aligned} \qquad (2)$$

where f_{Ti}, f_O and B_{Ti}, B_O are the atomic scattering factors and thermal parameters for the Ti and O atoms, respectively.[32] The first term[33] is the contribution from water of thickness d_w in the gallery and the other three are from the titanate sheets of lepidocrocite-type. Since the structure has a center of symmetry with respect to $y = 0$, only cosine terms are taken into account.

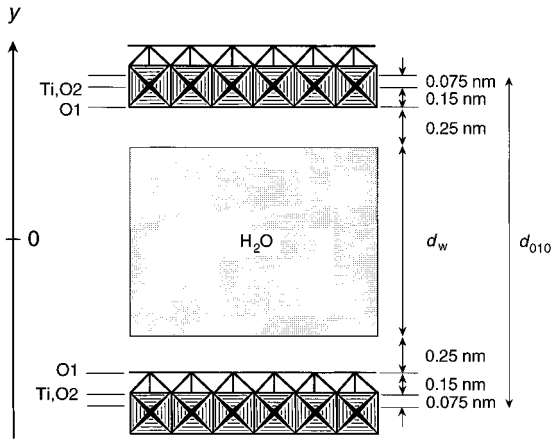

Atom	*n*	*y*
Ti	0.9125	$\pm d_{010}/2$ - 0.075
O1	1	$\pm d_{010}/2$ - 0.225
O2	1	$\pm d_{010}/2$ - 0.075
H_2O	$d_w/0.25$	$-d_w/2 \sim +d_w/2$ (continuous)

Figure 3. Structure model for the highly swollen titanate. Positional parameters are listed at the bottom.

The scattering power of the intersheet water was modeled as uniform electron density for liquid water.[34] Its magnitude, comparable to that of oxygen per 0.25 nm along the y axis, was derived as follows. The volume of water molecule is obtained as V/N_a (=2.99 × 10^{-2} nm^3) where V and N_a are the molar volume of liquid water at ambient conditions (=18 cm^3 = 1.8 × 10^{22} nm^3) and Avogadro's number (=6.022 × 10^{23} mol^{-1}), respectively. Division of this value with the cross-sectional area of the unit host layer (=0.114 nm^2 = 0.38 nm × 0.30 nm) gives the estimate of height (≈0.25 nm) for one water molecule within the unit area. This value is consistent with experimental data, that is, a difference in gallery heights of monolayer (~0.90 nm) and bilayer hydrates (~1.15 nm) which are formed in the alkali metal ion-exchange processes.[22]

There are three variable parameters for simulation; the intersheet separation, d_{010}, the number of the unit structure, N, and the thermal factors, B_{Ti}, B_O. The latter thermal parameters hardly affected the diffraction profile. Thus they were fixed as B_{Ti} = 0.05 nm^2 and B_O = 0.1 nm^2, which may be reasonable for this exceedingly thin system where larger positional disorder is likely in comparison with normal crystallites.

The typical simulated XRD profiles are shown in Figure 4. Table 1 summarizes the apparent spacing, line breadth, and relative intensity for the 0*k*0 reflections simulated for d_{010} = 11, 12 nm and N = 1, 2, 3. The comparable data extracted from the observed pattern are also tabulated. It is to be pointed out that the system with a very limited number of repeating unit cell produces diffraction peaks over an extended angular range, the peak top of which deviates from a normal position predicted from the Bragg equation. The departure is predominated by variations of the structure factor, F, and the Lorentz−polarization term and is dependent on N. The tendency is actually observed for the experimental data which are best fit with the simulation for d_{010} = 12 nm and N = 1.

One of the most discriminable parameters is the line width which also supports for the above conclusion N = 1. When N

(31) Although the 010 line was not visible at this stage being buried in a tail of the direct beam, it became perceptible as the intersheet distance contracted (see Figure 5).

(32) *International Tables for X-ray Crystallography*; The International Union of Crystallography, The Kynoch Press: Birmingham, England, 1968; pp 201−207.

(33) The integration can be transformed into the following term

$$= (f_O/0.25)\cdot(\sin(2\pi(\sin\theta/\lambda)\cdot d_w))/(2\pi\cdot\sin\theta/\lambda)$$

(34) The contribution from TBA ion is negligibly small because of its small scattering power, similar to that of water, and its low population in comparison with the number of water molecules.

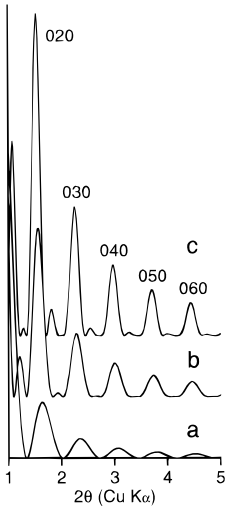

Figure 4. Simulated 0*k*0 diffraction patterns for the *N* parallel sheets with the spacing of 12 nm: (a) $N = 1$, (b) $N = 2$, (c) $N = 3$.

Table 1. Peak Profile Parameters for Simulated and Observed (0*k*0) Reflections

(a) Calculated for 11 nm

		010	020	030	040
$N = 1$	d (nm)[a]	9.03	5.00	3.49	2.67
	β (deg)[b]	0.351	0.370	0.382	0.385
	I[c]	580	100	37	20
$N = 2$	d (nm)	9.74	5.24	3.58	2.72
	β (deg)	0.222	0.251	0.262	0.270
	I	510	100	42	24
$N = 3$	d (nm)	10.2	5.36	3.63	2.74
	β (deg)	0.157	0.184	0.195	0.200
	I	460	100	44	27

(b) Calculated for 12 nm

		010	020	030	040
$N = 1$	d (nm)	9.12	5.38	3.76	2.88
	β (deg)	0.325	0.340	0.351	0.357
	I	620	100	36	19
$N = 2$	d (nm)	10.5	5.65	3.87	2.93
	β (deg)	0.206	0.220	0.242	0.249
	I	530	100	42	23
$N = 3$	d (nm)	10.9	5.77	3.92	2.96
	β (deg)	0.149	0.161	0.179	0.186
	I	490	100	44	26

(c) Observed

	010	020	030	040
d (nm)		5.4	3.8	2.9
β (deg)		0.35	0.35	0.36
I		100	40	20

[a] Spacing from peak top. [b] Full width at half maximum in 2θ (fwhm). [c] Integrated relative intensity.

≥ 2, fwhm quickly reduces to values much smaller than the observed ones. Note that instrumental broadening is negligible in the present case. The intrinsic angular breadth, $\beta_{\text{intrinsic}}$, can be obtained from the Warren's relation.[35]

$$\beta_{\text{intrinsic}}{}^2 = \beta_{\text{meas}}{}^2 - \beta_{\text{instr}}{}^2 \tag{3}$$

where β_{meas} and β_{instr} are experimentally measured width and instrumental resolution, respectively. Since $\beta_{\text{meas}}/\beta_{\text{instr}} = 5$ ($\beta_{\text{instr}} = 0.07°$; see Experimental Section), the correction is 2% which is within experimental error.

(35) Cullity, B. D. *Elements of X-ray Diffraction*: Addison-Wesley Publishing Company, Inc.: Reading, MA, 1957.

There are some other factors to be taken into account as possible sources of line broadening. The $N \geq 2$ system with (i) sheet bending or (ii) interstratification may yield broad diffraction lines which are comparable to the case for the paired assembly ($N = 1$). The sheet bending may be regarded as nonuniform distortion of the lattice. This random strain, η, contributes to broaden diffraction lines as follows:[35]

$$\beta_{\text{strain}} = 2\eta\tan\theta \tag{4}$$

The overall line width, β_{total}, is obtained as a sum of that arising from random strain, β_{strain}, and that from crystallite size, β_{cryst}:

$$\beta_{\text{total}} = \beta_{\text{strain}} + \beta_{\text{cryst}} \tag{5}$$

If the observed line breadth can be explained as a consequence from a crystallite of $N \geq 2$ with nonuniform distortion, a plot between $\beta_{\text{total}} - \beta_{\text{cryst}}$ and $\tan\theta$ should give a linear relationship with intercept 0. The term β_{cryst} can be taken from the values in Table 1. Since the proportionality is not obtained for the present data, the observed line width is not involved in such an effect. Although the exfoliated single sheets are likely to be flexible, the bended nanosheets do not contribute to the diffraction observed.

Another possibility, interstratification, is also excluded. Interference between more than two kinds of spacing could produce very broad diffraction peaks, especially when they are randomly stacked. However, in such a case, the series of basal reflections becomes irrational with large departure from integral indices. Furthermore, the line width is variable from one mixed-layered reflection to another. None of them was recognized. The observed deviation of peak positions from those based on the Bragg law is relatively small and can systematically be explained by the extremely small size of the crystallite, as mentioned above.

It is concluded from the above discussion that the diffraction observed is produced by a novel associated pair of nanosheets with an intersheet water cluster of thickness 12 nm. The detection of such a pairwise assembly as well as the large volume of amorphous component provides cogent proof for delamination into the single-layer level.

Dynamic Reassembling Process. It is of particular interest to follow how the reassembling propagates from the paired nanosheets. The conditioning at a relative humidity of 95% brought about a gradual diminution in intersheet spacing, as visualized by Figures 5 and 6a, which reached a constant value of ~2.7 nm after 12 h. Further shrinkage resulted by lowering the relative humidity (Figure 6b). The intersheet separation changed smoothly except for a jump at 50−70% humidity.[36] The discrete change, although it is not well-defined, suggests an intermediate hydrated phase with the intersheet separation of ~2.1 nm. The drying extinguished a large portion of the amorphous component observed at the beginning and resulted in a fairly well-ordered material (Figure 2c and Figure 5d) as a principal product, which can be identified as the TBA intercalated compound having the gallery height of 1.75 nm. Its XRD pattern was characteristic of irregular layer-to-layer registry,[37] indicating the turbostratic nature of the material.

The line profile analyses similar to those described above demonstrated that the restacking did not proceed very much until the intersheet spacing shrank to a value of ~3.0 nm. For example, the intermediate phase with the intersheet separation

(36) There is some hysteresis between drying and rehydration processes.

(37) The XRD data (Figure 2c) were recorded for the sample in filmlike texture as a result of the drying of the aggregate, in which $h*l$ reflections were suppressed due to preferred orientation. They were enhanced considerably for a well-ground sample.

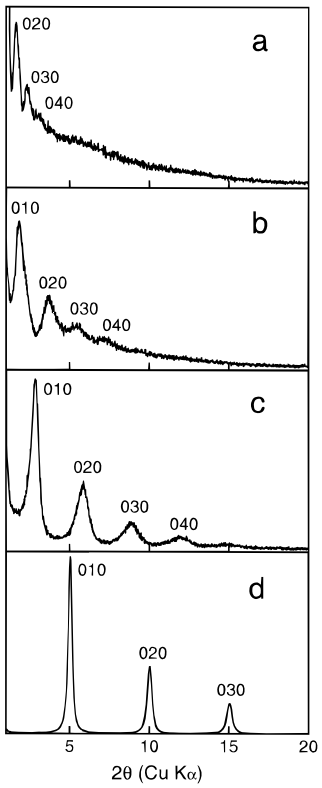

Figure 5. Change in X-ray diffraction patterns in the drying process of the colloidal aggregate: (a) immediately after separation from the liquid phase, (b) conditioned at a relative humidity of 95% for 7.7 h, (c) conditioned at a relative humidity of 95% for 11.7 h, (d) dried for 1 h at a relative humidity of 20%. The intensity scale in b is 20 times that in a. Temperature was regulated at 30 °C throughout.

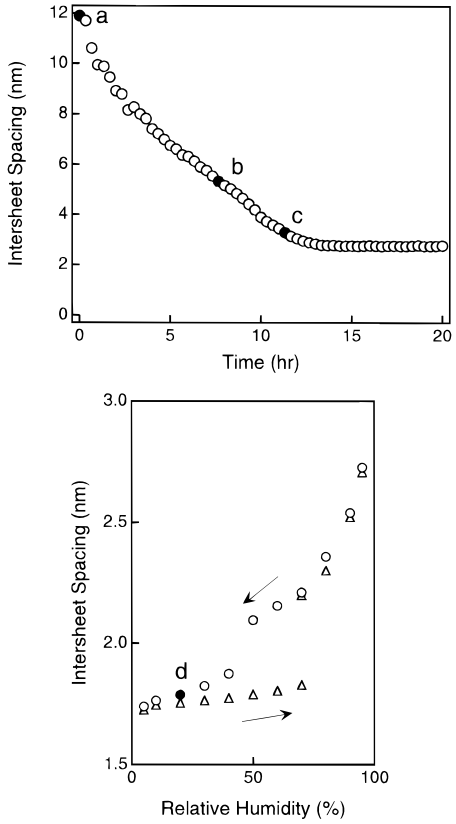

Figure 6. (a) Time dependence of the intersheet spacing at a constant relative humidity of 95%. (b) Change in spacing as a function of relative humidity. The product of process a was further examined in b with conditioning at various humidities (step: 10%) for 1 h: (○) downward, (△) upward. The data points designated by a−d correspond to the XRD patterns in Figure 5.

of ∼4.8 nm (b in Figure 5) was shown to be composed of two to three sheets.[38] The crystallites started to grow in terms of stacking number particularly with drying at lower humidity. The final TBA intercalated material was accounted for by a sequence of fourteen to fifteen sheets.

The mode of the reassembling process can be modified by a variety of parameters. Accelerated drying experiments conditioned at a lower humidity (<90%) frequently gave rise to segregation, or coexistence of two phases with different intersheet separations. This phenomena may be induced by heterogeneous drying, the speed being different between the surface and the inner region of the sample.

We can roughly estimate, based on eqs 1 and 2, how much of the nanosheets is crystallized at various stages. The observed intensity ratio of 020 lines for Figures 2b and 2c was ∼1/12. As described above, these two reflections stemmed from crystallites consisting of 2 and 14/15 sheets, respectively. On the other hand, the theoretical intensity for each crystallite is predicted to be 1/3.9. The discrepancy between these values means that population of the incoherent crystallites multiplied approximately three times in the course of the drying. It follows that the number of sheets initially crystallized as the paired species corresponds to a percent order (<3.9/12 × 2/14.5) of the total number, even if the sheets which remained amorphous at the final stage were neglected.

It can at least be concluded that the titanate was almost exfoliated to the elementary nanosheets. There are two explanations for the origin of the associated pair at the very beginning of drying. It may be present in the suspension or be evolved after separation from the liquid. It took a few minutes to load the colloidal aggregate onto a sample holder. This inevitably exposed the sample to air of ambient humidity, which may initiate crystallization. It is inconclusive at the present stage which possibility is the case. However, it is evident that reassembling of nanosheets was initiated from the pairwise species. The process involves an increase in population of the crystallites which grows in number of sheets but shrinks in terms of intersheet distance. In this sense, this species may be regarded as a kind of reassembling nucleus.

(38) The increment of the stacking number was not discrete but continuous. For example, there was not an explicit transition point along the time evolution curve (Figure 6a) where the fit changes in an obvious way from the pairwise assembly to three-sheet species. This may be explained by a mixture of a lower aggregate and higher ones the proportion of which changes steadily.

Discussion

The associated pair is novel in terms of its large intersheet spacing (>10 nm) as well as its very limited number (=2) of constituent nanosheets. The detection of such an elementary unit comprising only a pair of the nanosheets and its fundamental intersheet diffraction are of importance. Raw variation of the structure factor, strictly the square of it, is observed here as the wavy profile without being modified by the Laue function.

What drives the association and subsequent growth process? It is surprising that a pair of titanate sheets, more than 10 nm apart, arrange themselves in a parallel position. It seems unlikely that the paired nanosheets directly interact with each other from such a distance. We speculate that the osmotic pressure force is predominantly responsible for adopting such a configuration. Water in the intersheet region is progressively withdrawn by being in contact with the atmosphere at, more or less, an unsaturated humidty. When the intersheet separation

reaches ~3 nm, some cohesive force between the sheets starts exerting itself, probably through electrostatic interaction via the TBA cation. This promotes the abrupt increase in stacking number after this point.

It is of great interest to compare the hydration behavior of the titanate with that of smectite clay minerals since both systems exhibit similar swellings which are very unusual in comparison with other classes of inorganic layered compounds. Dehydrated smectities take up moisture to be swollen in a stepwise fashion. Four distinct stages of hydration involving 0−3 water layers in the galleries are formed as a function of relative humidity.[39] Similar stepwise expansion is recognized for the titanate in the present study. The TBA intercalated titanate, or the final product of drying, lost water upon heating at 200 °C without collapse of the lamellar structure. The gallery height contracted from 1.75 to 1.45 nm with dehydration. As pointed out above, the ~2.1-nm phase was suggested from the shape of the curve in Figure 6b. The differences between these spacings are 0.30−0.35 nm, which is consistent with expansion for one additional water layer. Thus the 1.45-, 1.75-, and ~2.1-nm phases are attributable for zero-, mono-, and bilayer hydrate structures, respectively. The presence of trilayer hydrate is inconclusive from the present data. The stepwise hydration behavior is common for a variety of layered compounds, e.g., the titanates[20b,21,22b,24] and transition metal disulfides[40] having alkali metal ions as guests.

The unusual feature for the titanate and smectities is that beyond the modest hydration above, they undergo a much higher degree of expansion where their intersheet spacings exceed 10 nm. It is to be noted that hydration with expansion of this magnitude has seldom been observed except for the materials discussed here.[41] This type of solvation for smectities, which is achieved by being immersed in water, is referred to as the osmotic swelling.[39a,42] However, their diffraction patterns are generally poor exhibiting one broad line, which is interpreted as statistical distribution of the intersheet spacing. This is in contrast to the well-defined feature in the present case with several higher order reflections which are from a single spacing. The difference may be associated with the lateral dimensions for the dispersed single sheets. The lateral size for titanate nanosheets studied here ought be in micrometer or submicrometer scale.[30] On the other hand, typical clay minerals are much smaller, probably being tens of nanometers.[43] This dimension is in comparable order of the intersheet separation of osmotic expansion, which may facilitate introduction of various stacking disorder.

It should be pointed out that there are still ambiguous points for full understanding of the swelling. The experimental data discussed here for both systems may not necessarily reflect comparable phenomenon. The osmotic swelling has been studied by adding the appropriate amount of water to powdery clay minerals, which represents the forward process from a normal stacked structure to clloidal single sheets. The restacking behavior from dispersed single sheets of clay has not been reported. Thus conclusive discussion must await similar study for clay minerals to this experiments.

The present study has demonstrated the complete exfoliation to the single sheets and clarified the transient structural and chemical changes during the reassembling process. In these reactions, the nanosheets behave as individual molecular entities rather than as assemblies or crystals. "Inorganic macromolecules" classically refer to compounds with covalent frameworks such as silicates (mica, quartz) and carbon (graphite, diamond). However, their attributes are not of molecules but of crystals. The colloidal nanosheets can be regarded as genuine macromolecules in the sense that they behave individually. A similar nature may be found for some inorganic gels intermediately polymerized in sol-gel processes. Molecule-like aspects have been pointed out or predicted for some low-dimensional inorganic materials.[11,44,45] The data described here may represent such features.

The nature of "single-layer colloids" has not been thoroughly uncovered, especially with respect to their chemistry as macromolecules. The parallel data to those in this study have not been reported even for colloids of clay minerals which have been investigated extensively for decades. The in situ diffraction study presented here can be applied to a variety of other "single-layer colloids", which will provide much information on these new classes of "inorganic macromolecules" and consequently lead to better control of their chemistry.

Conclusion

The layered protonic titanate, $H_xTi_{2-x/4}\square_{x/4}O_4{\cdot}H_2O$, was exfoliated into single layers by being treated with the TBA hydroxide solution, which is the first example of a single-layer titanate. The delaminated nanosheets were restacked again upon drying, which was initiated from the novel pairwise association. The number of stacked sheets increased from 2 for the paired assembly to 14/15 for the TBA intercalated compound as the final dried product, through the process of which the intersheet separation contracted from the unusually high degree of hydration (>10 nm) to the usual value of 1.75 nm. The dynamic reassembling process particularly in terms of sheet-to-sheet interaction reveals macromolecule-like aspects for the individual nanosheets. These features may be common for other "single-layer colloids" including clay minerals and may give a clue to understanding their inherent nature as two-dimensional macromolecules.

Experimental Section

Reagents and Materials. A titanium dioxide and a cesium carbonate (99.99% purity; Rare Metallic Co. Ltd) were used as supplied. All the other chemicals were of reagent grade. Milli-Q filtered water (Millipore Co., >15 MΩ cm^{-1}) was used throughout.

The layered protonic titanate, $H_xTi_{2-x/4}\square_{x/4}O_4{\cdot}H_2O$ ($x = 0.70$), was prepared by the procedures described before.[22] The parent Cs compound, $Cs_xTi_{2-x/4}\square_{x/4}O_4$,[46] was obtained by repeating twice the heat treatment (800 °C, 20 h) of a stoichiometric mixture of Cs_2CO_3 and TiO_2. The interlayer Cs ions were extracted by stirring ~50 g of $Cs_xTi_{2-x/4}\square_{x/4}O_4$ in a 1 mol dm^{-3} HCl solution (2 dm^3). After three

(39) (a) MacEwan, D. M. C.; Wilson, M. J. *Crystal Structures of Clay Minerals and Their X-Ray Identification*; Brindley, G. W., Brown, G., Eds.; Mineralogical Society: London, 1980; pp 206−211. (b) Glaeser, R.; Méring, J. *C. R. Hebd. Séances Acad. Sci., Paris* **1968**, *267*, 436−466. (c) Moore, C. M.; Hower, J. *Clays Clay Miner.* **1986**, *34*, 379−384. (d) Watanabe, T.; Sato, T. *Clay Sci.* **1988**, *7*, 129−138. (e) Yamada, H.; Nakazawa, H.; Hashizume, H.; Shimomura, S.; Watanabe, T. *Clays Clay Miner.* **1994**, *42*, 77−80.

(40) Schöllhorn, R. *Intercalation Chemistry*; Whittingham, M. S., Jacobson, A. J., Eds.; Academic Press: New York, 1982.

(41) Although several classes of layered compounds have been reported to undergo delamination to single sheets, or infinite swelling, organized hydrated structures with exceptionally high degree of expansion have not been found except for clay minerals and the present material.

(42) (a) Norrish, K. *Discuss. Faraday Soc.* **1954**, *18*, 120−134. (b) Foster, W. R.; Savins, J. E.; Waite, J. M. *Clays Clay Miner.* **1955**, *3*, 296−316. (c) Fukushima, Y. *Clays Clay Miner.* **1984**, *32*, 320−326.

(43) Güven, N. *Hydrous Phyllosilicates*; Bailey, S. W., Ed.; Mineralogical Society of America: Washington, DC, 1988.

(44) Rouxel, J. *Chim. Scr.* **1988**, *28*, 33−40.

(45) Stein, A.; Keller, S. W.; Mallouk, T. E. *Science* **1993**, *259*, 1558−1564.

(46) (a) Hervieu, M.; Raveau, B. *Rev. Chim. Min.* **1981**, *18*, 642−649. (b) Grey, I. E.; Madsen, I. C.; Watts, J. A.; Bursill, L. A.; Kwiatkowska, J. *J. Solid State Chem.* **1985**, *58*, 350−356. (c) Grey, I. E.; Li, C.; Madsen, I. C.; Watts, J. A. *J. Solid State Chem.* **1987**, *66*, 7−19.

cycles of acid exchange, the solid was washed with copious water to remove excess acid, filtered, and then dried in air. The resulting protonic oxide was white polycrystalline powder, the grain of which was micrometer-sized platy microcrystals.

Preparation of the Colloidal Suspensions by Exfoliation of the Titanate. A weighed amount (0.025−1.0 g) of $H_xTi_{2-x/4}\square_{x/4}O_4\cdot H_2O$ was shaken (150 rpm) with 100 cm^3 of an aqueous solution of TBA hydroxide, which produced the stable colloidal suspensions. The TBA concentration was 0.02−0.5 mol dm^{-3}. The resulting dispersion was translucent to opalescent, depending on the titanate content. The suspension of typical composition (0.4 wt %, molar ratio of TBA in solution/H^+ in $H_xTi_{2-x/4}\square_{x/4}O_4\cdot H_2O$ = 5) was examined in depth in this study.

X-ray Diffraction. The XRD data for the colloidal suspensions were collected by a powder diffractometer (Rigaku Rint 2000S) with graphite-monochromatized Cu Kα radiation (λ = 0.15405 nm). The system is based on Bragg-Bretano parafocussing geometry with a goniometer circle radius of 185 nm. Slits such as divergence of 0.5°, scattering of 0.5°, and receiving of 0.15 mm were employed to obtain good data at a low angular range. The diffractometer is equipped with the horizontal sample stage in a humidity/temperature controllable chamber. The instrumental resolution (fwhm) is 0.07° in 2θ at the low angular range (2θ < 5°) which was estimated using data for 1-tetradecanol.

The XRD data for the suspension itself did not give significant information on the titanate due to an enormous halo from water. Then the suspension was centrifuged (15000 rpm, 30 min) to separate a glue-like material which should be an aggregate of the nanosheets. The information on the wet colloid itself, which should be close to the natural state, was acquired by suppressing evaporation of water. The subsequent drying process was also monitored under conditions where the evaporating speed was controlled.

In order to obtain a precise profile, absorption correction was applied to the data using the following equation.[35]

$$I_{corr} = C\cdot I_{obs}\cdot\frac{\sin\theta_{diff}}{\mu(\sin\theta_{inc}+\cos\theta_{diff})}\cdot[1-\exp(-\mu t(\mathrm{cosec}\theta_{inc}+\mathrm{cosec}\theta_{diff}))] \quad (6)$$

where I_{obs}, I_{corr} and θ_{inc}, θ_{diff} are observed, corrected intensities and incident, diffracted angles, respectively. C is constant. The linear absorption coefficient, μ, is 22−23 cm^{-1} for the structural model with the intersheet distance of 11−12 nm. The sample thickness, t, is 0.05 cm.

Acknowledgment. The authors are grateful to Dr. Mitsuko Onoda of the National Institute for Research in Inorganic Materials for her useful discussion on XRD data.

JA960073B